

# End-to-end Learning for OFDM: From Neural Receivers to Pilotless Communication

Fayçal Ait Aoudia, *Member, IEEE*, and Jakob Hoydis, *Senior Member, IEEE*

## Abstract

Previous studies have demonstrated that end-to-end learning enables significant shaping gains over additive white Gaussian noise (AWGN) channels. However, its benefits have not yet been quantified over realistic wireless channel models. This work aims to fill this gap by exploring the gains of end-to-end learning over a frequency- and time-selective fading channel using orthogonal frequency division multiplexing (OFDM). With imperfect channel knowledge at the receiver, the shaping gains observed on AWGN channels vanish. Nonetheless, we identify two other sources of performance improvements. The first comes from a neural network (NN)-based receiver operating over a large number of subcarriers and OFDM symbols which allows to significantly reduce the number of orthogonal pilots without loss of bit error rate (BER). The second comes from entirely eliminating orthogonal pilots by jointly learning a neural receiver together with either superimposed pilots (SIPs), linearly combined with conventional quadrature amplitude modulation (QAM), or an optimized constellation geometry. The learned geometry works for a wide range of signal-to-noise ratios (SNRs), Doppler and delay spreads, has zero mean and does hence not contain any form of superimposed pilots. Both schemes achieve the same BER as the pilot-based baseline with around 7 % higher throughput. Thus, we believe that a jointly learned transmitter and receiver are a very interesting component for beyond-5G communication systems which could remove the need and associated control overhead for demodulation reference signals (DMRSs).

## Index Terms

Autoencoder, end-to-end learning, geometric shaping, superimposed pilots, orthogonal frequency division multiplexing, frequency-selective fading, channel estimation

## I. INTRODUCTION

End-to-end learning has attracted a lot of attention in recent years and it is considered to be a promising technology for future wireless communication systems [1], [2]. Its key idea is to

The authors are with Nokia Bell Labs, 91620 Nozay, France ({faycal.ait\_aoudia, jakob.hoydis}@nokia-bell-labs.com).

implement the transmitter, channel, and receiver as a single neural network (NN), referred to as an autoencoder, that is trained to achieve the highest possible information rate [3], [4]. Since its first application to wireless communications [5], end-to-end learning has been extended to other fields including optical wireless [6] and optical fiber [7]. However, most of the literature is either simulation-based on simple channel models, such as additive white Gaussian noise (AWGN) or Rayleigh block fading (RBF), or experimental, but performed in static environments [3], [8]. Such setups do not account for the Doppler and delay spread encountered in practical wireless systems that lead to variations of the channel response in both time and frequency. The evaluation of end-to-end learning on more realistic channel models is overlooked in the existing literature but critical to bring the technology from theory to practice.

For the reasons mentioned above, we evaluate in this work the benefits of end-to-end learning for orthogonal frequency division multiplexing (OFDM)-based communication over a time- and frequency-selective fading channel model. We consider a Kronecker structure for the tempo-spectral correlation, using Jakes' Doppler power spectrum and 3rd Generation Partnership Project (3GPP) power delay profiles. This model allows us to accurately and conveniently control the Doppler and delay spreads to evaluate the communication performance in different scenarios. It was already shown in previous work that end-to-end learning enables significant shaping gains on AWGN and static channels [4]. However, we have observed that these gains vanish on realistic channels with imperfect channel knowledge at the receiver. Therefore, we need to find other ways to increase performance for such channels. We focus especially on the potential of end-to-end learning to eliminate the need for orthogonal pilot signals, i.e., pilot signals transmitted on dedicated resource elements (REs), such as demodulation reference signal (DMRS) in 5G New Radio (5G NR), by jointly optimizing parts of the transmitter and receiver. Two approaches are presented to achieve this goal. The first consists in learning superimposed pilots (SIPs) that are linearly combined with the quadrature amplitude modulation (QAM) modulated baseband symbols on the OFDM grid. The second approach is more radical and consists in learning a constellation and associated bit labeling which are used to modulate coded bits on all REs. The learned constellation is forced to have zero mean to avoid an unwanted direct current (DC) offset. As a side-effect, it can also not be interpreted as a constellation with superimposed pilots. In both approaches, the NN used at the receiver has a fully convolutional structure and operates jointly on multiple subcarriers and OFDM symbols, as in [9], [10].

For benchmarking, we have implemented two strong baseline receivers which rely on linear

minimum mean square error (LMMSE) channel estimation with perfect tempo-spectral covariance matrix knowledge and iterative estimation, demapping, and decoding (IEDD), respectively. We have also evaluated the performance gains that can be obtained by leveraging only the neural receiver together with standard QAM and pilot patterns from 5G NR. Our results show that such a receiver enables significant bit error rate (BER) improvements in scenarios with high mobility and/or when sparse pilot patterns are used, although the channel code is not at all leveraged as for IEDD. These results concur with the observations made in [9] regarding the robustness of a neural receiver with respect to a decreased number of pilots. As a consequence, an NN-based receiver with QAM and sparse orthogonal pilot patterns from 5G NR enables worthwhile throughput gains. Regarding joint optimization of the transmitter and receiver, our results demonstrate that the two approaches we introduce achieve BERs similar to the ones achieved by the NN-based receiver with QAM and orthogonal pilots for various speeds and delay spreads. As a consequence, end-to-end learning enables additional throughput gains in the range from 4 % to 8 %, depending on the scenario, by removing all orthogonal pilots.

### *Related literature*

End-to-end learning over OFDM channels was first considered in [11], in which the autoencoder is assumed to operate over individual REs. This limitation prevents the receiver from taking advantage of the tempo-spectral correlation of the OFDM channel. This approach is extended towards the learning of a peak-to-average power ratio (PAPR) reduction scheme in [12]. In [13], one-bit quantization of the received OFDM signal is considered, and joint optimization of a precoder and decoder is performed to enable reconstruction of the transmitted signal.

A handful of studies have focused on neural receivers for OFDM systems in the recent years. In [9], a neural receiver made of dense layers is optimized to jointly process several OFDM symbols, with the first symbol carrying pilots. It is observed that the neural receiver is more robust than conventional receivers when fewer pilots or no cyclic prefix is transmitted. A large residual convolutional NN is considered in [10] which operates over a large number of subcarriers and OFDM symbols. BERs close to what can be achieved with perfect channel knowledge are observed over realistic 3GPP channel models. It is also shown that such a neural receiver is more robust against interference compared to traditional approaches.

The goal of our work is to investigate what additional benefits can be achieved from end-to-end learning when a neural receiver is used. More specifically, the reduction or complete suppression

of pilots is explored in this work. There exists a rich literature on this topic, involving schemes that typically require detection algorithms of prohibitive complexity (see, e.g., [14], [15] and references therein).

The rest of this manuscript is structured as follows: Section II presents the channel model and the receiver baselines against which the NN-based approaches are compared. Section III introduces the neural receiver and end-to-end schemes that enable communication without orthogonal pilots. Section IV presents the simulations results while Section V concludes the paper.

*Notations:* Boldface upper-case (lower-case) letters denote matrices (column vectors).  $\mathbb{R}$  ( $\mathbb{C}$ ) is the set of real (complex) numbers;  $j$  is the imaginary unit,  $()^*$  the complex conjugate operator.  $\ln(\cdot)$  denotes the natural logarithm and  $\log_2(\cdot)$  the binary logarithm.  $\mathcal{CN}(\mathbf{m}, \mathbf{S})$  is the complex multivariate Gaussian distribution with mean  $\mathbf{m}$  and covariance  $\mathbf{S}$ . The  $(i, k)$  element of a matrix  $\mathbf{X}$  is denoted by  $X_{i,k}$ . The  $k^{th}$  element of a vector  $\mathbf{x}$  is  $x_k$  and  $\text{diag}(\mathbf{x})$  is a diagonal matrix with  $\mathbf{x}$  as diagonal. The operators  $()^H$  and  $\text{vec}()$  denote the Hermitian transpose and vectorization, respectively. For two matrices  $\mathbf{X}$  and  $\mathbf{Y}$ , their Hadamard and Kronecker products are denoted by  $\mathbf{X} \circ \mathbf{Y}$  and  $\mathbf{X} \otimes \mathbf{Y}$ , respectively. Random variables are denoted by capital italic font, e.g.,  $X$ , with realizations  $x$ . Random vectors are denoted by capital bold calligraphic font, e.g.,  $\mathcal{X}$ , with realizations  $\mathbf{x}$ .  $I(X; Y)$ ,  $p(y|x)$  and  $p(x, y)$  represent respectively the mutual information, conditional probability, and joint probability distribution of  $X$  and  $Y$ .

## II. CHANNEL MODEL AND RECEIVER BASELINES

We start by introducing the channel model which is used throughout this work. We will then detail two baseline receiver algorithms for performance benchmarking with the machine learning-based approaches which are presented in Section III.

### A. Channel model

We consider an OFDM system with  $n_S$  subcarriers that operates on transmission time intervals (TTIs) (or blocks) of  $n_T$  consecutive OFDM symbols, forming a frame. After cyclic-prefix removal and discrete Fourier transform at the receiver, the corresponding complex-baseband channel model is

$$\mathbf{Y} = \mathbf{H} \circ \mathbf{X} + \mathbf{W} \quad (1)$$

where  $\mathbf{Y} \in \mathbb{C}^{n_S \times n_T}$  is the received signal,  $\mathbf{H} \in \mathbb{C}^{n_S \times n_T}$  the channel matrix,  $\mathbf{X} \in \mathbb{C}^{n_S \times n_T}$  the matrix of transmitted symbols, and  $\mathbf{W} \in \mathbb{C}^{n_S \times n_T}$  additive white complex Gaussian noise with

variance  $\sigma^2$  per element. Depending on the transmission scheme, some elements of  $\mathbf{X}$  can be used for pilot symbols while the others carry modulated symbols according to a constellation, e.g., QAM or a learned constellation. It is also possible that the elements of  $\mathbf{X}$  carry modulated symbols together with superimposed pilots, as explained later. For all schemes, the transmitted symbols are assumed to have an average energy equal to one, i.e.,  $\mathbb{E}\{|X_{i,k}|^2\} = 1$ . Let us denote by  $\mathbf{h} = \text{vec}(\mathbf{H}) \in \mathbb{C}^n$  the vectorization of  $\mathbf{H}$ , where  $n = n_S n_T$ . The vector  $\mathbf{h}$  is sampled from a complex Gaussian distribution with zero mean and covariance matrix  $\mathbf{R} \in \mathbb{C}^{n \times n}$ . This assumption is valid if the number of propagation paths is large enough and some conditions on the path gains are satisfied [16]. The matrix  $\mathbf{R}$  determines the temporal and spectral correlation of the OFDM channel. Both are assumed to be separable, i.e., the matrix  $\mathbf{R}$  can be written as the Kronecker product of a frequency correlation matrix  $\mathbf{R}_F \in \mathbb{C}^{n_S \times n_S}$  and a time correlation matrix  $\mathbf{R}_T \in \mathbb{C}^{n_T \times n_T}$ , according to

$$\mathbf{R} = \mathbf{R}_F \otimes \mathbf{R}_T. \quad (2)$$

The received signal power is assumed to be uniformly distributed with respect to the angle of arrival at the receiver. Such a model corresponds to a Clarke-Jakes power angular spectrum which is a reasonable assumption if the receiver is immersed in the propagation clutter [17]. The corresponding time correlation matrix is given by [18]

$$[\mathbf{R}_T]_{i,k} = J_0 \left( 2\pi \frac{v}{c} f_c \Delta_T (i - k) \right), \quad 1 \leq i, k \leq n_T \quad (3)$$

where  $J_0(\cdot)$  is the zero-order Bessel function of the first kind,  $c$  [m s<sup>-1</sup>] the speed of light,  $v$  [m s<sup>-1</sup>] the receiver speed relative to the transmitter,  $f_c$  [Hz] the carrier frequency and  $\Delta_T$  [s] the duration of an OFDM symbol. Regarding the frequency correlation, it can be computed given a delay spread  $D_s$  [s] and a power delay profile composed of  $L$  *normalized* delays  $\tau_l$  and corresponding powers  $S_l$ , for  $l = 1, \dots, L$ , according to [17]

$$[\mathbf{R}_F]_{i,k} = \sum_{l=1}^L S_l e^{j2\pi\tau_l D_s \Delta_F (i-k)}, \quad 1 \leq i, k \leq n_S \quad (4)$$

where  $\Delta_F = \frac{1}{\Delta_T}$  [Hz] is the subcarrier spacing.

Generating channel realizations  $\mathbf{h}$  can be done by sampling from  $\mathcal{CN}(\mathbf{0}, \mathbf{R})$ . This can be achieved by filtering a non-correlated Gaussian vector  $\mathbf{n} \sim \mathcal{CN}(\mathbf{0}, \mathbf{I}_n)$  as

$$\mathbf{h} = \mathbf{U} \mathbf{\Lambda}^{\frac{1}{2}} \mathbf{n} \quad (5)$$

where  $\mathbf{R} = \mathbf{U} \mathbf{\Lambda} \mathbf{U}^H$  is the eigenvalue decomposition of  $\mathbf{R}$ .

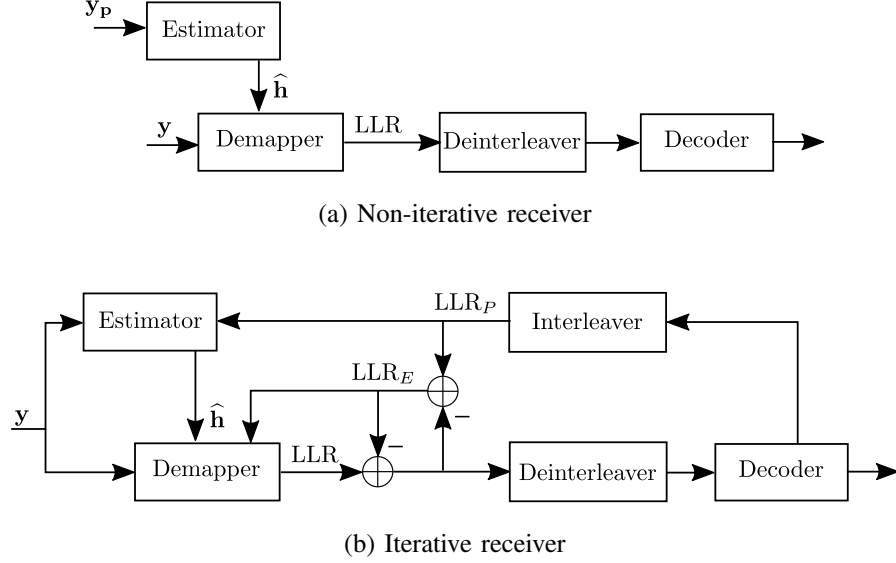


Fig. 1: Considered baselines for the receiver

Two receiver baselines are considered in this work. The first one performs LMMSE channel estimation based on transmitted pilots, followed by soft-demapping assuming Gaussian noise, as illustrated in Fig. 1a. The second baseline also relies on LMMSE channel estimation and Gaussian demapping, but leverages IEDD [19]. These two baselines are detailed in the rest of this section. They are respectively referred to as the *non-iterative* and *iterative* baselines.

### B. LMMSE channel estimation and Gaussian demapping

We denote by  $\mathbf{P} \in \mathbb{C}^{n_S \times n_T}$  the pilot matrix, whose entry  $P_{i,k}$  is zero if the RE on the  $i^{th}$  subcarrier and  $k^{th}$  time slot is carrying data, or equal to the pilot value otherwise. Let  $n_P$  be the number of pilot-carrying REs which are considered for channel estimation. For these REs, we can re-write the channel transfer function (1) in vectorized form as

$$\mathbf{y}_P = \mathbf{\Pi} (\text{diag}(\mathbf{p})\mathbf{h} + \mathbf{w}) \quad (6)$$

where  $\mathbf{p} = \text{vec}(\mathbf{P})$ ,  $\mathbf{w} = \text{vec}(\mathbf{W})$ , and  $\mathbf{\Pi}$  is the  $n_P \times n$  matrix which selects only the elements carrying pilot symbols. Assuming knowledge of the channel correlation matrix  $\mathbf{R}$  at the receiver, the LMMSE channel estimate is (e.g., [20, Lemma B.17])

$$\hat{\mathbf{h}} = \mathbf{R} \text{diag}(\mathbf{p})^H \mathbf{\Pi}^H (\mathbf{\Pi} (\text{diag}(\mathbf{p})\mathbf{R} \text{diag}(\mathbf{p})^H + \sigma^2 \mathbf{I}_n) \mathbf{\Pi}^H)^{-1} \mathbf{y}_P. \quad (7)$$

Using this result, the received signal in (1), which incorporates both pilots and data, can be re-written in vector form as

$$\mathbf{y} = \text{diag}(\hat{\mathbf{h}})\mathbf{x} + \underbrace{\text{diag}(\tilde{\mathbf{h}})\mathbf{x} + \mathbf{w}}_{\triangleq \tilde{\mathbf{w}}} \quad (8)$$

where  $\tilde{\mathbf{h}} = \mathbf{h} - \hat{\mathbf{h}}$  is the channel estimation error with correlation matrix  $\tilde{\mathbf{R}} \in \mathbb{C}^{n \times n}$ , given as

$$\tilde{\mathbf{R}} = \mathbb{E} \left\{ \tilde{\mathbf{h}} \tilde{\mathbf{h}}^H \right\} = \mathbf{R} - \mathbf{R} \text{diag}(\mathbf{p})^H \mathbf{\Pi}^H \left( \mathbf{\Pi} \left( \text{diag}(\mathbf{p}) \mathbf{R} \text{diag}(\mathbf{p})^H + \sigma^2 \mathbf{I}_n \right) \mathbf{\Pi}^H \right)^{-1} \mathbf{\Pi} \text{diag}(\mathbf{p}) \mathbf{R} \quad (9)$$

and  $\tilde{\mathbf{w}}$  is the sum of noise and residual interference due to imperfect channel estimation.

Soft-demapping is performed assuming that  $\tilde{\mathbf{w}}$  is Gaussian.<sup>1</sup> Let us denote by  $m$  the number of bits per channel use, by  $\mathcal{C} = \{c_1, \dots, c_{2^m}\}$  the constellation, and by  $\mathcal{C}_{i,0}$  ( $\mathcal{C}_{i,1}$ ) the subset of  $\mathcal{C}$  which contains all constellation points with the  $i^{\text{th}}$  bit label set to 0 (1). The log-likelihood ratio (LLR) for the  $i^{\text{th}}$  bit ( $i \in \{1, \dots, m\}$ ) of the  $k^{\text{th}}$  RE ( $k \in \{1, \dots, n\}$ ) is computed as follows:

$$\text{LLR}(k, i) = \ln \left( \frac{\sum_{c \in \mathcal{C}_{i,1}} \exp \left( -\frac{1}{\tilde{\sigma}_k^2} |y_k - \hat{h}_k c|^2 \right)}{\sum_{c \in \mathcal{C}_{i,0}} \exp \left( -\frac{1}{\tilde{\sigma}_k^2} |y_k - \hat{h}_k c|^2 \right)} \right) \quad (10)$$

where  $\tilde{\sigma}_k^2 = \mathbb{E} \{ \tilde{w}_k \tilde{w}_k^* \} = \tilde{R}_{k,k} + \sigma^2$  for  $k = 1, \dots, n$ . Whenever  $k$  corresponds to the index of a pilot symbol, no LLR value is computed. After deinterleaving, the LLRs are fed to a channel decoding algorithm (e.g., belief propagation) which computes predictions of the transmitted bits.

### C. Iterative channel estimation, demapping and decoding

The key idea of IEDD is to leverage the channel code to improve channel estimation and demapping. Instead of running the estimator, demapper, and decoder once, as illustrated in Fig. 1a, IEDD consists of running the estimator, demapper, and a few iterations of the decoder in an iterative manner, as illustrated in Fig. 1b. At each iteration, the LLRs generated by the decoder are used as prior knowledge on the transmitted bits by the estimator and demapper. Formally, at each iteration, prior information is assumed to be available to the channel estimator for each bit  $i \in \{1, \dots, m\}$  of each RE  $k \in \{1, \dots, n\}$  in the form of LLRs denoted by  $\text{LLR}_P(k, i)$ . From these LLRs, a prior distribution  $P_{X_k}$  is computed for each transmitted data symbol  $x_k \in \mathcal{C}$  as follows:

$$[P_{X_k}(c_1), \dots, P_{X_k}(c_{2^m})] = \text{softmax} \left( \sum_{i=1}^m c_1^{(i)} \text{LLR}_P(k, i), \dots, \sum_{i=1}^m c_{2^m}^{(i)} \text{LLR}_P(k, i) \right) \quad (11)$$

<sup>1</sup>This is typically not true as  $\text{diag}(\tilde{\mathbf{h}})\mathbf{x}$  is not Gaussian.

where  $c_u^{(i)} \in \{0, 1\}$  refers to the value of the  $i^{th}$  bit label of the constellation symbol  $c_u$ , and the softmax function is defined as  $\text{softmax}(l_1, \dots, l_{2^m}) = \left[ \frac{\exp(l_1)}{\sum_{i=1}^{2^m} \exp(l_i)}, \dots, \frac{\exp(l_{2^m})}{\sum_{i=1}^{2^m} \exp(l_i)} \right]$ . A derivation of all the equations related to the IEDD baseline can be found in Appendix-A. The prior distribution is over the constellation set  $\mathcal{C}$  from which  $x_k$  takes its value. At the first iteration, no prior information is available and the prior LLRs are therefore set to zero. Regarding the pilot symbols, the prior distribution always corresponds to the deterministic distribution with probability one for the pilot symbol and zero for any other symbol, i.e., if the symbol  $p \in \mathbb{C}$  is transmitted as a reference signal on the  $k^{th}$  RE, then  $P_{X_k}(X_k = p) = 1$  and  $P_{X_k}(X_k \neq p) = 0$ .

Given the prior distributions  $P_{X_k}$ , the LMMSE channel estimate is

$$\hat{\mathbf{h}}' = \mathbf{R} \text{diag}(\bar{\mathbf{x}})^H (\mathbf{R} \circ \mathbb{E}\{\mathbf{xx}^H\} + \sigma^2 \mathbf{I})^{-1} \mathbf{y} \quad (12)$$

where  $\bar{x}_k \triangleq \mathbb{E}_{P_{X_k}}\{x_k\}$  and

$$\mathbb{E}\{\mathbf{xx}^H\}_{i,k} = \begin{cases} \mathbb{E}_{P_{X_k}}\{|x_k|^2\} & \text{if } i = k \\ \mathbb{E}_{P_{X_i}}\{x_i\} \mathbb{E}_{P_{X_k}}\{x_k^*\} & \text{otherwise,} \end{cases} \quad (13)$$

which assumes that the symbols forming  $\mathbf{x}$  are not correlated.<sup>2</sup> Equation (12) is a form of *data-aided channel estimation* as prior information on the data symbols is used in addition to the pilot symbols to perform channel estimation. The correlation matrix of the estimation error is

$$\tilde{\mathbf{R}}' = \mathbf{R} - \mathbf{R} \text{diag}(\bar{\mathbf{x}})^H (\mathbf{R} \circ \mathbb{E}\{\mathbf{xx}^H\} + \sigma^2 \mathbf{I})^{-1} \text{diag}(\bar{\mathbf{x}}) \mathbf{R}. \quad (14)$$

Demapping leverages the *extrinsic information* generated by the decoder, which can be intuitively seen as the additional information generated by the decoder only, and is obtained by subtracting its input from its output [19], as illustrated in Fig. 1b. The extrinsic information is available in the form of LLRs, which is denoted by  $\text{LLR}_E(k, i)$  for the  $i^{th}$  bit transmitted in the  $k^{th}$  RE. The LLR for the  $i^{th}$  bit of the  $k^{th}$  RE computed by the demapper is

$$\text{LLR}(k, i) = \ln \left( \frac{\sum_{c \in \mathcal{C}_{i,1}} \exp \left( -\frac{1}{\tilde{\sigma}_k'^2} \left| y_k - \hat{h}_k c \right|^2 + \sum_{l=1}^m c^{(l)} \text{LLR}_E(k, l) \right)}{\sum_{c \in \mathcal{C}_{i,0}} \exp \left( -\frac{1}{\tilde{\sigma}_k'^2} \left| y_k - \hat{h}_k c \right|^2 + \sum_{l=1}^m c^{(l)} \text{LLR}_E(k, l) \right)} \right) \quad (15)$$

where  $\tilde{\sigma}_k'^2 = \tilde{R}'_{k,k} + \sigma^2$ , for  $k = 1, \dots, n$ . As shown in Fig. 1b, only the extrinsic information generated by the demapper is forwarded to the decoder, which is obtained by subtracting from the LLRs (15) the prior information  $\text{LLR}_P$ .

<sup>2</sup>This might not be true in practice as the channel code introduces redundancy.



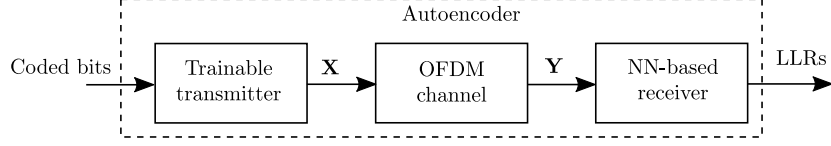


Fig. 2: Autoencoder-based communication system

### III. END-TO-END LEARNING FOR OFDM

End-to-end learning of communication systems [5] consists in implementing a transmitter, channel, and receiver as a single NN referred to as an autoencoder, as illustrated in Fig. 2, and jointly optimizing the trainable parameters of the transmitter and receiver for a specific channel model. In our setting, training aims at minimizing the total binary cross-entropy (BCE) [bit frame<sup>-1</sup>], defined as

$$\mathcal{L} \triangleq - \sum_{k \in \mathcal{N}_D} \sum_{i=1}^m \mathbb{E}_{b_{k,i}, \mathbf{y}} \{ \log_2 (Q_{k,i} (b_{k,i} | \mathbf{y})) \} \quad (16)$$

where  $\mathcal{N}_D$  is the set of size  $n_D$  of indexes of REs carrying data symbols,  $b_{k,i}$  is the  $i^{th}$  bit transmitted in the  $k^{th}$  resource element, and  $Q_{k,i}(\cdot | \mathbf{y})$  is the receiver estimate of the posterior distribution on the  $i^{th}$  bit transmitted in the  $k^{th}$  RE given the channel output  $\mathbf{y}$ . Since (16) is numerically difficult to compute, it is estimated through Monte Carlo sampling as

$$\mathcal{L} \approx \frac{1}{S} \sum_{l=1}^S \sum_{k \in \mathcal{N}_D} \sum_{i=1}^m \left\{ \log_2 \left( Q_{k,i} \left( b_{k,i}^{[l]} | \mathbf{y}^{[l]} \right) \right) \right\} \quad (17)$$

where  $S$  is the batch size, i.e., the number of samples used to estimate  $\mathcal{L}$ , and the superscript  $[l]$  is used to refer to the  $l^{th}$  sample forming a batch. The total BCE (16) can be rewritten as

$$\mathcal{L} = n_D m - R \quad (18)$$

with  $R$  defined as

$$R \triangleq \sum_{k \in \mathcal{N}_D} \sum_{i=1}^m I(B_{k,i}; \mathcal{Y}) - \sum_{k \in \mathcal{N}_D} \sum_{i=1}^m \mathbb{E}_{\mathbf{y}} \{ \text{D}_{\text{KL}} (P_{B_{k,i}}(\cdot | \mathbf{y}) || Q_{k,i}(\cdot | \mathbf{y})) \} \quad (19)$$

where  $B_{k,i}$  is the random variable corresponding to the  $i^{th}$  transmitted bit in the  $k^{th}$  RE,  $\mathcal{Y}$  is the random variable corresponding to the received symbols,  $\text{D}_{\text{KL}}(\cdot || \cdot)$  is the Kullback–Leibler (KL) divergence, and  $P_{B_{k,i}}(\cdot | \mathbf{y})$  is the *true* posterior distribution on the transmitted bits given the channel output  $\mathbf{y}$ . The first term in (19) is the maximum information rate that can be achieved assuming an ideal bit-metric decoding (BMD) receiver and depends only on the transmitter and

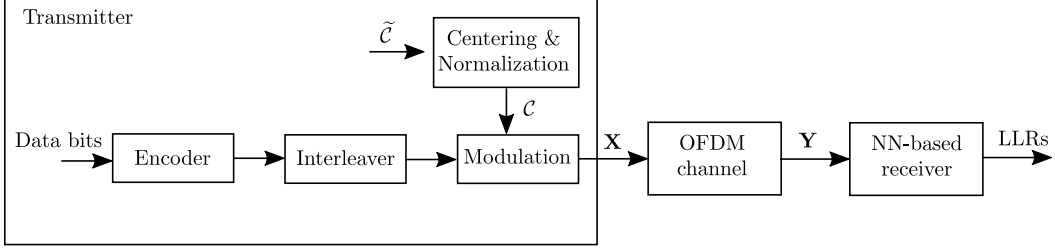


Fig. 3: End-to-end system with trainable constellation and receiver

channel. The second term in (19) is the rate loss caused by an imperfect receiver, which equals zero if the receiver computes the true posterior distribution of the transmitted bits. Interestingly, in accordance to the following proposition,  $R$  is an achievable rate assuming a mismatched BMD receiver is used. Therefore, by minimizing  $\mathcal{L}$ , one actually maximizes the achievable rate  $R$ .

**Proposition 1.**  *$R$  is an achievable rate in the sense of the standard definition [21, §8.5].*

*Proof.* See Appendix-B. □

Training of the transmitter typically involves joint optimization of the constellation geometry and bit labeling [4]. Such an approach is adopted in this work and extended to OFDM channels in Section III-A. Moreover, a centered constellation is learned, assuming that no orthogonal pilots are transmitted. This avoids an unwanted DC offset and removes the throughput loss due to the transmission of reference signals that carry no data. Motivated by previous observations that training of end-to-end systems over fading channels leads to the learning of constellations that embed SIPs [5], [22], we also consider the learning of an SIP scheme based on conventional QAM in Section III-B. The architecture of the NN-based receiver is detailed in Section III-C.

#### A. Learning of geometric shaping and bit-labeling

The system architecture we have adopted in this work is depicted in Fig. 3. On the transmitter side, the trainable parameters consist of a set denoted by  $\tilde{C}$  of  $2^m$  complex numbers corresponding to the constellation points. The constellation used for transmitting data is obtained by centering and normalizing  $\tilde{C}$ , i.e.,

$$c = \frac{\tilde{C} - \frac{1}{2^m} \sum_{c \in \tilde{C}} c}{\sqrt{\frac{1}{2^m} \sum_{c \in \tilde{C}} |c|^2 - \left| \frac{1}{2^m} \sum_{c \in \tilde{C}} c \right|^2}}. \quad (20)$$

Normalization of the constellation ensures it has unit average power, while centering forces the constellation to have zero mean and therefore avoids an undesired DC offset. Centering the constellation as done in (20) prevents learning of embedded SIPs. As no orthogonal pilots are transmitted, the receiver can only exploit the constellation geometry to reconstruct the transmitted bits. Compared to previous work such as [4], a single constellation is learned, which is used for all signal-to-noise ratios (SNRs), Doppler, and delay spreads. On the receiver side, an NN that operates on multiple subcarriers and OFDM symbols is leveraged, whose architecture is detailed in Section III-C. As in [4], training of the end-to-end systems is done on the total BCE estimated by (17).

### B. Learning of superimposed pilots

Typical communication systems rely on pilot patterns which describe how pilots and data symbols are scattered over the REs within a frame. Such pilots are said to be orthogonal as each RE is either carrying a modulated data symbol or a reference signal. SIPs adopt a different approach by splitting the energy available for each RE between a reference signal and a data symbol. Therefore, compared to orthogonal pilots, all REs are used to transmit modulated data symbols. Formally, the transmitted symbol on the  $i^{th}$  subcarrier and on the  $k^{th}$  time slot is

$$X_{i,k} = \underbrace{\sqrt{1 - A_{i,k}} \tilde{X}_{i,k}}_{\text{Data}} + \underbrace{\sqrt{A_{i,k}} P_{i,k}}_{\text{Pilot}} \quad (21)$$

where  $\tilde{X}_{i,k}$  is the modulated data symbol that takes values in a constellation set  $\mathcal{C}$  with zero mean,  $A_{i,k} \in [0, 1]$  controls the fraction of energy allocated to the reference signal (the rest being allocated to the data symbol), and  $P_{i,k}$  is a predefined reference signal. Equation (21) can be written in matrix form as

$$\mathbf{X} = \sqrt{\mathbf{1} - \mathbf{A}} \circ \tilde{\mathbf{X}} + \sqrt{\mathbf{A}} \circ \mathbf{P} \quad (22)$$

where  $\mathbf{1}$  is the matrix full of ones and the square root is taken elementwisely.

We now propose to jointly optimize the pilot allocation matrix  $\mathbf{A}$  and the NN-based receiver to maximize the achievable rate (19). Our approach differs from previous work on deep learning of pilot patterns [23]–[25] in several ways. Firstly, we focus on SIPs, whereas prior art focuses on orthogonal pilots. Secondly, the referenced papers consider learning of a channel estimator to reduce the mean squared error (MSE) between the true channel and the estimate. In this work, we train on the achievable rate (19) as this is the metric of interest when optimizing communication

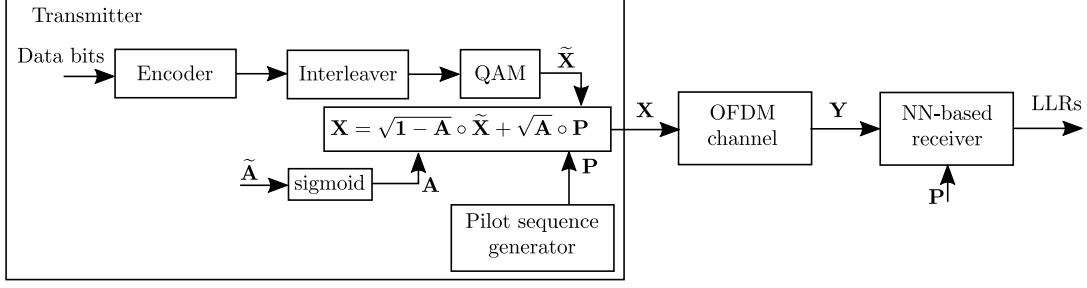


Fig. 4: QAM with superimposed pilots

systems from end-to-end. That way, the system is optimized to learn the right amount of energy which should be allocated to pilots, whereas previous approaches required a pruning step and regularization as training on the MSE leads to most of the energy being allocated to pilots, as the system is not inclined to free resources for data transmission.

The considered system is shown in Fig. 4. The pilot allocation matrix  $\mathbf{A}$  is obtained by elementwisely taking the sigmoid of an unconstrained matrix  $\tilde{\mathbf{A}}$ , whose coefficients are optimized at training. To ensure that the transmitted signal has zero average energy, the pilot matrix  $\mathbf{P}$  is formed by randomly sampling a binary phase-shift keying (BPSK) constellation according to a pseudo-random sequence with zero mean. As shown in Fig. 4, the so-generated pilot matrix is fed as an additional input to the NN-based receiver, whose architecture is detailed thereafter.

### C. Receiver architecture

The architecture of the NN implementing the receiver is shown in Fig. 5. It is a convolutional residual NN [26] that takes as input the received baseband channel samples  $\mathbf{Y}$  of dimension  $n_S \times n_T$ , and outputs a 3-dimensional tensor of LLRs of dimension  $n_S \times n_T \times m$  that is fed to the channel decoder after a deinterleaving step. The NN hence substitutes the estimator and demapper shown in Fig. 1a. The first layer  $\mathbb{C}2\mathbb{R}$  converts the complex-valued input tensor of dimension  $n_S \times n_T$  into a real-valued 3-dimensional tensor of dimension  $n_S \times n_T \times 2$  by stacking the real and imaginary parts into an additional dimension. No iterative scheme is involved as in the IEDD baseline. Separable convolutional layers are used to reduce the number of weights, without incurring significant loss of performance. Table I provides details on the NN implementing the receiver. All convolutional layers use zero-padding to ensure that the dimensions of the output are the same as the ones of the input. The two separable convolutional layers in a ResNet block

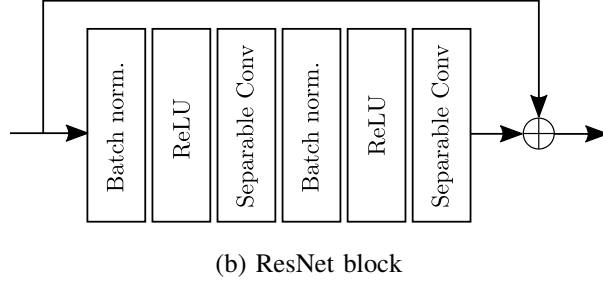
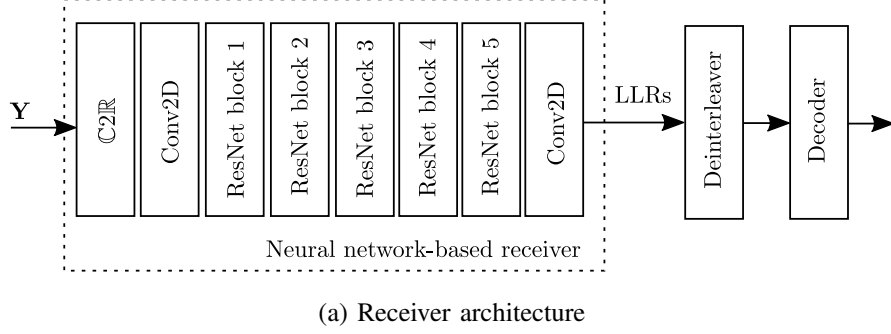


Fig. 5: Architecture of the NN-based receiver

Layer	Channels	Kernel size	Dilatation rate
Input Conv2D	64	(3,3)	(1,1)
ResNet block 1	128	(7,7)	(7,2)
ResNet block 2	128	(7,5)	(7,1)
ResNet block 3	128	(5,3)	(1,2)
ResNet block 4	128	(3,3)	(1,1)
ResNet block 5	128	(3,3)	(1,1)
Output Conv2D	$m$	(1,1)	(1,1)

TABLE I: Architecture details of the NN implementing the receiver

(Fig. 5b) share the same dimensions. A similar but somewhat larger architecture was used in [10] with great success.

#### IV. SIMULATION RESULTS

We will now present the results of the simulations we have conducted to evaluate the machine learning-based schemes introduced in the previous section. We start by explaining the training and evaluation setup. Then, we benchmark the NN-based receiver introduced in Section III-C

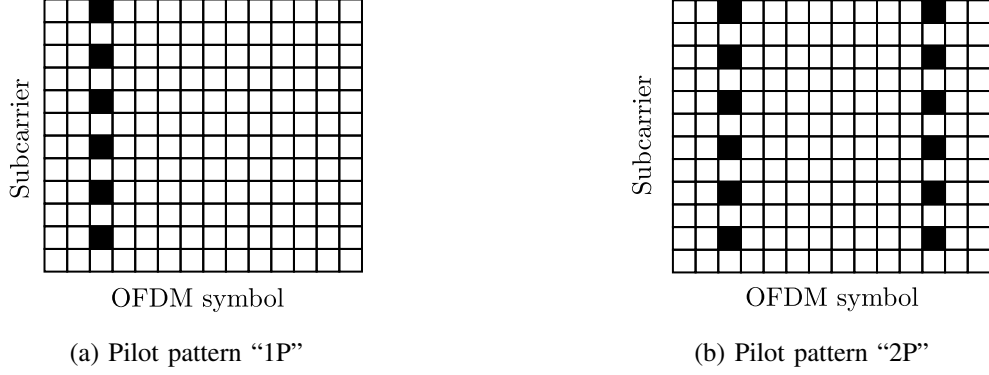


Fig. 6: Pilot patterns from 5G NR used in simulations

against the non-iterative and iterative baselines presented in Section II, considering conventional QAM at the transmitter with pilots patterns from 5G NR and over different speeds. The end-to-end learning schemes introduced in Sections III-A and III-B are then compared to conventional approaches leveraging orthogonal pilot patterns.

#### A. Evaluation setup

The channel model introduced in Section II-A was considered to train the end-to-end systems and to evaluate them against multiple baselines. In addition to the non-iterative and iterative baselines, perfect channel knowledge at the receiver was also considered as it provides an upper-bound on the achievable performance. Table II shows the parameters used to train and evaluate the machine learning-based approaches. Three speed ranges were considered, referred to as “low”, “medium”, and “high” that are within the range from 0 to  $35 \text{ m s}^{-1}$ . Training of the machine learning-based approaches was done over the entire speed range and over the delay spread range from 10 to 1000 ns. The TDL-B and TDL-C 3GPP power delay profiles were used for training, whereas the TDL-A profile was used for evaluation to ensure that no overfitting to a particular power delay profile has occurred. A Gray-labeled QAM with modulation order 64 ( $m = 6$ ) was used. For a given OFDM frame with realization  $\mathbf{H}$ , the energy per bit to noise power spectral density ratio is defined as

$$\frac{E_b}{\sigma^2} \triangleq \frac{1}{\rho} \frac{\sum_{i=1}^{n_S} \sum_{k=1}^{n_T} |H_{i,k}|^2}{nmr\sigma^2} \quad (23)$$

assuming  $\mathbb{E}\{|X_{i,k}|^2\} = 1$  for all REs  $(i, k)$ , and where  $\rho$  is the ratio of REs carrying data symbols within a frame (the rest of the REs being used for pilots) and  $r$  is the code rate. Two

Parameter	Symbol (if any)	Value
Number of OFDM symbols	$n_T$	14 (1 slot)
Number of subcarriers	$n_S$	72 (6 PRBs)
Frequency carrier	$f_c$	2.6 GHz
Subcarrier spacing	$\Delta_f$	15 kHz
Noise variance	$\sigma^2$	-20 dB
Learning rate	(None)	$10^{-3}$
Batch size for training	$S$	100 frames
Power delay profiles for training	(None)	TDL-B and TDL-C
Power delay profiles for evaluation	(None)	TDL-A
Bit per channel use	$m$	6 bit
Code length	(None)	1944 bit
Code rate	$r$	$\frac{2}{3}$
Low speed range	(None)	0 to $5.5 \text{ m s}^{-1}$
Medium speed range	(None)	14.7 to $20.3 \text{ m s}^{-1}$
High speed range	(None)	29.5 to $35 \text{ m s}^{-1}$
Speed range used for training	(None)	0 to $35 \text{ m s}^{-1}$
Delay spread range for evaluation	(None)	70 to 140 ns
Delay spread range used for training	(None)	10 to 1000 ns

TABLE II: Parameters used for training and evaluation

pilot patterns from 5G NR were considered, which are shown in Fig. 6. The first one has pilots on only one OFDM symbol (Fig. 6a,  $\rho = \frac{162}{168}$ ), whereas the second one has extra pilots on a second OFDM symbol (Fig. 6b,  $\rho = \frac{156}{168}$ ), which makes it more suitable to high mobility scenarios. These two pilot patterns are referred to as “1P” and “2P”, respectively.

A standard IEEE 802.11n low-density parity-check (LDPC) code of length 1944 bit and with rate  $\frac{2}{3}$  was used [27]. Decoding was done with conventional belief-propagation, using 40 iterations for the non-iterative baseline and machine learning-based approaches. Regarding the iterative baseline, 4 iterations were performed, each involving a channel estimation and soft-demapping step as well as 10 iterations of belief-propagation. Each transmitted OFDM frame contained 3 codewords and was filled up with randomly generated padding bits. Interleaving was performed within individual frames.

The NN-based receiver operates on the entire frame. For fairness, the channel estimations (7) and (12) for the non-iterative and iterative baselines, respectively, are also performed on the entire

frame. This involves the multiplication and inversion of matrices of dimension  $1008 \times 1008$ . Moreover, it requires knowledge of the channel correlation matrix  $\mathbf{R}$ , which depends on the the Doppler and delay spread. However, the receiver typically does not have access to this information, and assuming it to be available would lead to an unfair comparison with the NN-based receiver which is not fed with the Doppler and delay spread. Therefore, a unique correlation matrix has been estimated by sampling  $10^6$  random channel realizations over the entire speed and delay spread ranges, and using the TDL-B and TDL-C power delay profiles. The so-obtained correlation matrix estimate was used to implement the baselines.

### *B. Evaluation of the NN-based receiver*

In this section, we will focus only on a learned receiver as described above using conventional QAM and pilot patterns from 5G NR (see Fig. 6). An NN-based receiver was optimized for each pilot pattern. By training only the receiver on the total BCE (16), one minimizes the KL divergence between the posterior distribution on the transmitted bits implemented by the NN-based receiver and the true posterior distribution, as the first term in (19) depends only on the transmitter and channel. In other words, the receiver is optimized to compute values close to the true posterior distribution on the transmitted bits given the channel output.

The first column of Fig. 7 shows the BERs achieved by the evaluated schemes with the pilot pattern 1P for the three speed ranges. As one can see, only the NN-based receiver achieves BERs within 2 dB from the perfect channel knowledge bound for all speed ranges. At low speeds (Fig. 7a), the NN-based receiver enables BERs less than 0.5 dB from the perfect channel knowledge bound. All schemes experience higher BERs as the speed increases (Fig 7c and Fig. 7e). However, conventional baselines are less robust to higher speeds compared to the neural receiver. This is especially true for the iterative scheme, which enables significant gains at low speeds compared to the non-iterative approach, but which vanish at high speeds.

Similarly, the second column of Fig. 7 compares the BERs of all schemes using the 2P pilot patten. As one can see, all schemes have BERs close to the perfect channel knowledge limit. At high speeds (Fig. 7f), the iterative baseline achieves the lowest BERs, closely followed by the neural receiver which outperforms the non-iterative baseline. Similar simulations where conducted considering three delay spread ranges. The results revealed no significant impact of the delay spread on the relative performance, and are therefore not shown in this paper.



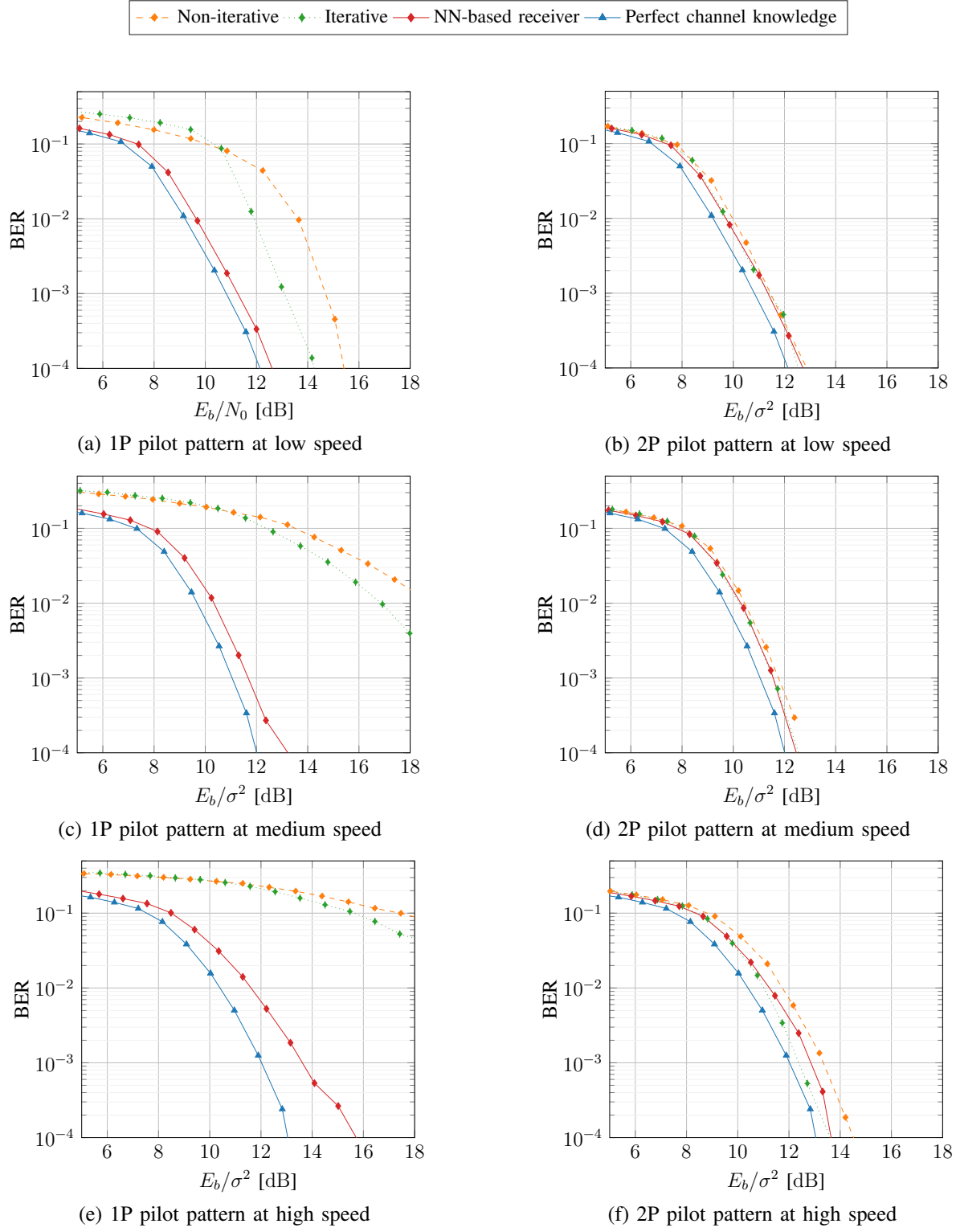


Fig. 7: BER achieved by the evaluated receivers for different ranges of speed

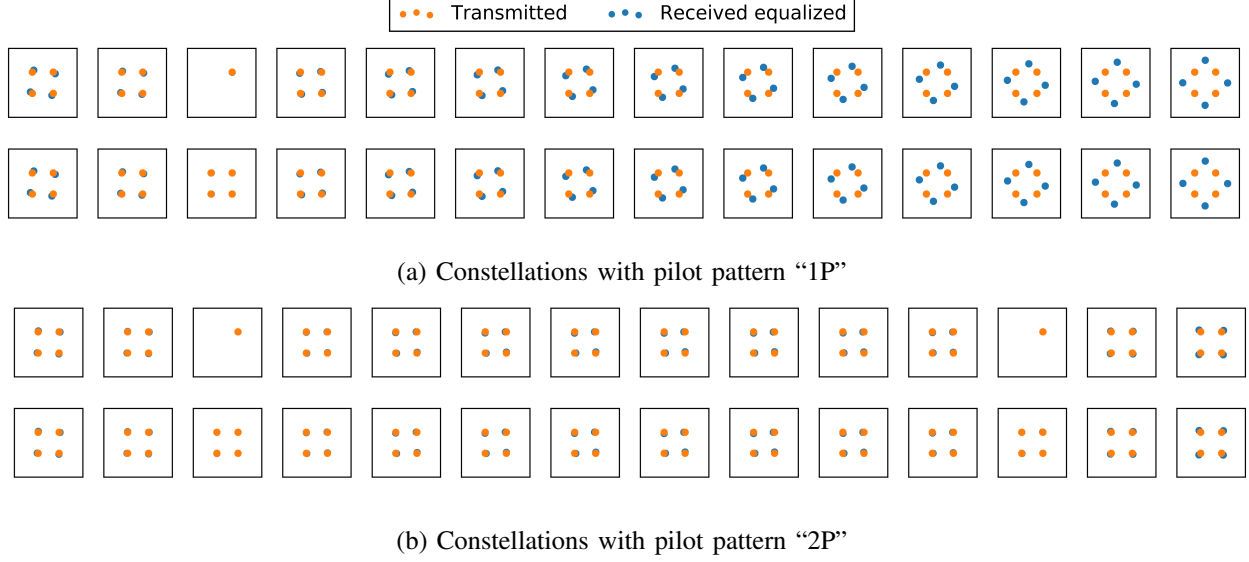


Fig. 8: Equalized received symbols at high speed, medium delay spread, and infinite SNR. The effect of a single channel realization is shown. The RE containing a single point corresponds to the pilots.

To get insight into why conventional baselines fail when using the 1P pilot pattern, Fig. 8 shows the equalized received symbols using the non-iterative baseline for one slot and 2 subcarriers in the high speed scenario (i.e., corresponding to the BERs of Fig. 7e and Fig. 7f). This figure was generated considering the effect of a single channel realization, and assuming an infinite SNR, such that only the effect of channel aging appears. A quadrature phase-shift keying (QPSK) constellation was used for readability. The REs in which a single point is visible correspond to pilots. As one can see, when the 1P pilot pattern is used (Fig. 8a), equalized symbols match the ground-truth constellation for REs located near the pilots. However, for REs located further away from the reference signals, i.e., located at the end of the slot, channel aging causes significant mismatch between the true channel coefficients and the estimated ones, despite the infinite SNR. This effect is amplified by the channel noise, and leads to the high error rates observed when using such a pilot pattern. One can therefore suppose that the NN-based receiver is able to better correct the effects of channel aging compared to conventional baselines, by possibly leveraging the data-carrying symbols for improved channel estimation. When using the 2P pilot pattern (Fig. 8b), the presence of a second pilot at the end of the slot reduces the effect of channel aging, leading to much lower error rates.

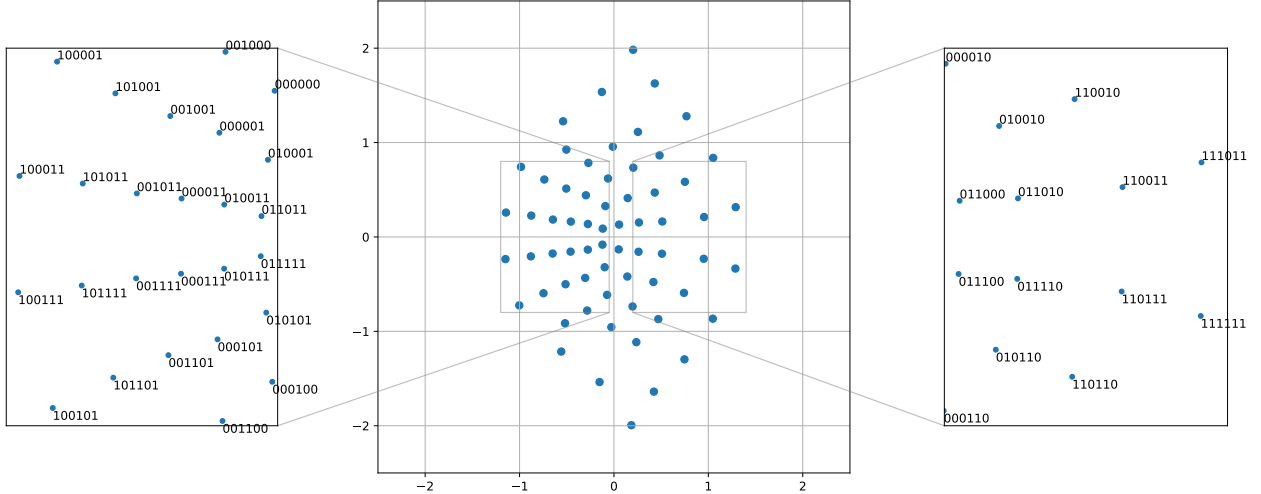


Fig. 9: Constellation obtained from end-to-end learning which eliminates the need for orthogonal or superimposed pilots

From these results, one can conclude that NN-based receivers are mostly beneficial in high-speed scenarios and/or for sparse pilot patterns. We have observed that we can drastically reduce the number of pilots, in some cases down to a single subcarrier carrying two pilots, without significant increase of BER. A similar observation was made in [9] regarding the robustness to a lower number of pilots. Although lower BERs can be achieved by transmitting more pilots with conventional baselines, this comes at the cost of lower throughput. Therefore, an NN-based receiver can enable higher throughputs. The next section demonstrates that joint optimization of the transmitter and receiver enables further throughput gains by completely removing the need for orthogonal reference signals.

### C. Evaluation of end-to-end learning

The two end-to-end schemes presented in Sections III-A and III-B are evaluated in this section. In addition to the previously introduced baselines, joint optimization of the constellation geometry and bit labeling, assuming perfect channel knowledge at the receiver is also considered.

Fig. 9 shows the constellation and labeling obtained by training the end-to-end system introduced in Section III-A, and referred to as the geometric shaping (GS) scheme. One can see that the learned constellation has a unique horizontal axis of symmetry. Moreover, a form of Gray labeling was learned, such that points next to each other differ by one bit.

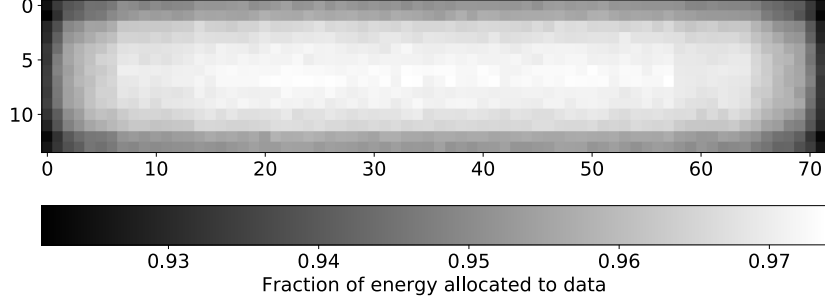


Fig. 10: SIP allocation learned by the end-to-end system

Regarding the QAM-SIP scheme introduced in Section III-B, the pilot allocation obtained by optimizing the system is shown in Fig. 10. One can see that for all REs, less than 10% of the available energy is allocated to SIPs. The REs located at the edges of the frame have a higher ratio of their energy allocated to SIPs compared to the other REs, especially, the first and last subcarriers of the frame. However, overall, the variation across the frame is rather small. Thus, optimizing a single energy-level used by all the REs could be sufficient and reduce implementation complexity.

The first column of Fig. 11 shows the BERs achieved by the various schemes. For readability, QAM with the non-iterative (Section II-B) and iterative (Section II-C) receivers are not shown, as these schemes achieve similar or higher BERs than QAM with the NN-based receiver (Section IV-B). As one can see, when perfect channel knowledge at the receiver is assumed, optimization of the constellation geometry and labeling only makes little difference. The GS and QAM-SIP schemes achieve BERs similar to the ones of QAM with orthogonal pilots and the NN-based receiver. This is the case regardless of which orthogonal pilot pattern is used. Moreover, these results hold for the three considered speed ranges.

The benefits of achieving low BERs without the requirement of transmitting orthogonal pilots, as allowed by the GS and QAM-SIP schemes, is that it enables higher *goodput*, as shown in the second column of Fig. 11. The non-iterative receiver baseline was omitted as it achieves similar or worse performance than the iterative one. The goodput measures the number of bits per frame successfully received, and is defined by

$$\text{Goodput} \triangleq r \rho m n (1 - \text{BER}) \quad (24)$$

where  $n$  is the number of REs forming a frame, and  $\rho$  is the ratio of data carrying REs within a physical resource block (PRB) ( $\rho = 1$  for GS, QAM-SIP, and when perfect channel knowledge

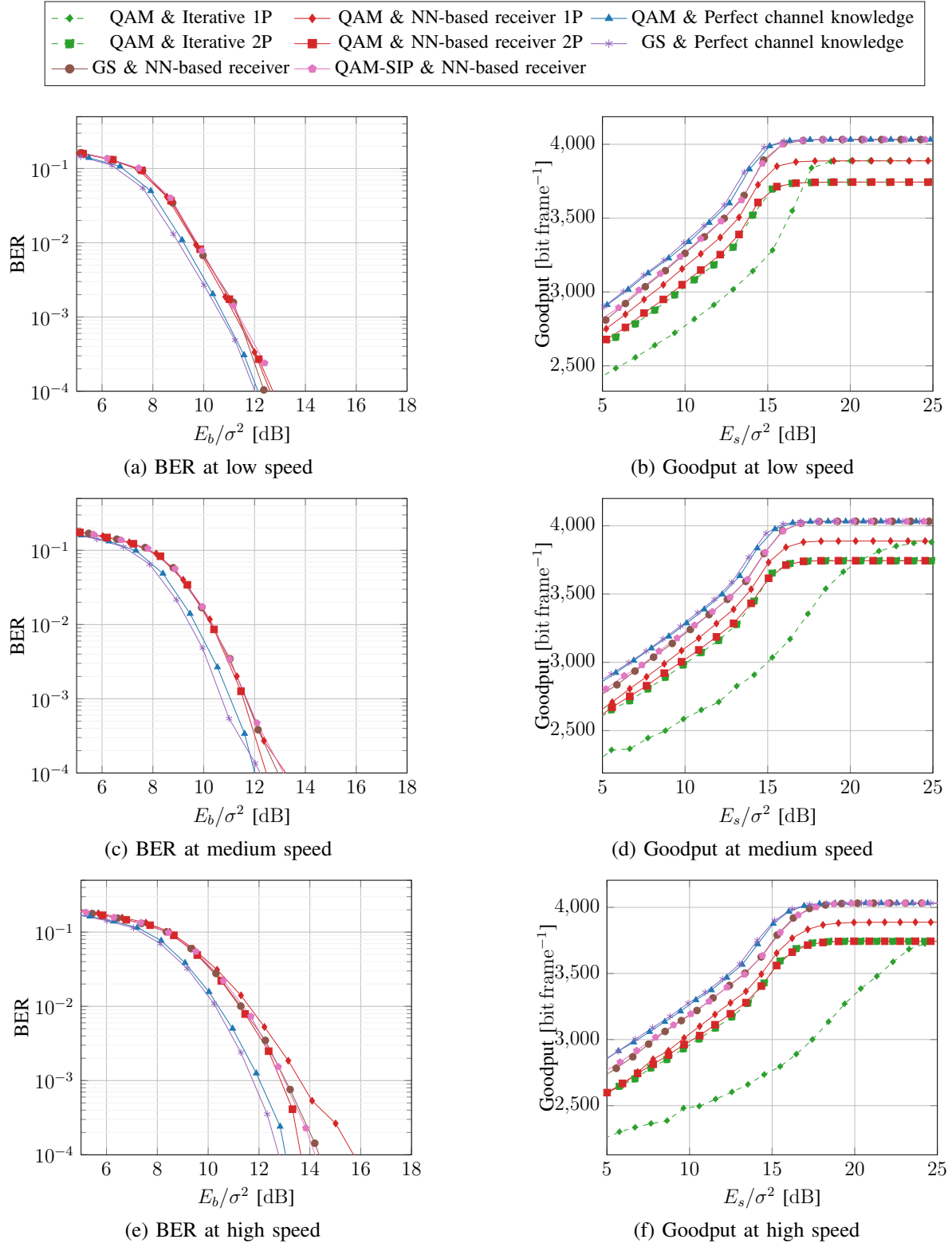


Fig. 11: BER and goodput achieved by the evaluated schemes for different ranges of speed

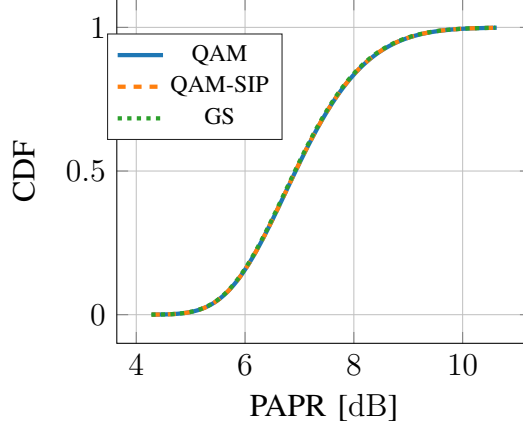


Fig. 12: CDF of the PAPR

is assumed at the receiver,  $\rho = \frac{162}{168}$  when the orthogonal 1P pilot pattern is used, and  $\rho = \frac{156}{168}$  when the orthogonal 2P pilot pattern is used). Moreover, because the goodput accounts for the unequal average number of information bits transmitted per RE among the different schemes through the parameter  $\rho$ , it is plotted with respect to the energy per symbol to noise power spectral density ratio, defined as

$$\frac{E_s}{\sigma^2} \triangleq \frac{\sum_{i=1}^{n_S} \sum_{k=1}^{n_T} |H_{i,k}|^2}{n\sigma^2}. \quad (25)$$

These plots show that an NN-based receiver with QAM and orthogonal pilots enables close to 25 % higher goodput than the receiver baselines when the 1P pilot pattern is used at high speeds (Fig. 11f). One can see that for all the considered speed ranges, the GS and QAM-SIP schemes achieve goodput close to the one with perfect channel knowledge at the receiver, especially when  $E_s/\sigma^2$  is higher than 15 dB. The orthogonal pilot-based schemes saturate at lower values as some of the REs are allocated to reference signals. The additional gains enabled by end-to-end learning range from 4 % to 8 % depending on which pilot pattern is used by the baselines. Therefore, one can conclude from these results that the majority of the gains enabled by end-to-end learning can be achieved by leveraging an NN-based receiver with sparse pilot patterns. However, joint optimization of the transmitter and receiver is required if one wants to achieve the highest possible gains by suppressing all orthogonal pilots.

#### D. PAPR study

We conclude this section by evaluating the PAPR incurred by the evaluated approaches. Fig. 12 shows the cumulative distribution function (CDF) of the PAPR of QAM, QAM-SIP, and GS. For each scheme,  $7 \times 10^6$  OFDM symbols were randomly generated, and the inverse discrete Fourier transform of each symbol was taken to obtain time domain symbols. The PAPR CDF was generated based on these time domain symbols. As one can see, QAM-SIP and GS lead to nearly the same distributions of the PAPR as conventional QAM. From these results, these two approaches should not lead to higher distortion of the transmitted signal than conventional QAM. This is encouraging towards implementation and use of the proposed schemes.

### V. CONCLUSION

We have evaluated the performance of a neural receiver considering an OFDM channel model that includes frequency selectivity and channel aging. Evaluations were performed for different speed ranges. Our results show that when a few orthogonal pilots are used, a neural receiver operating over multiple subcarriers and OFDM symbols enables significantly lower BERs. The gains are more pronounced in high mobility scenarios. We have then demonstrated how joint optimization of the transmitter and neural receiver allows reliable symbol detection without the need for orthogonal pilots. This permits throughput gains as no RE is wasted for the transmission of reference signals. Suppression of orthogonal pilots can be achieved either by learning SIPs that are linearly combined with QAM modulated data carrying symbols, or by learning a zero mean constellation that is used to modulate the data. Because the learned constellation is forced to have zero mean, the second approach does not leverage any form of reference signal (orthogonal or superimposed). Moreover, our simulations reveal that both schemes do not negatively affect the PAPR compared to conventional QAM. We therefore believe that such schemes could be part of beyond-5G communication systems, as they allow unprecedented throughput and reliability, while removing the need for DMRSs. Apart from throughput gains, pilotless transmissions could remove the control signaling overhead related to the choice of the best suitable pilot pattern, as the learned constellations and SIP patterns work for any SNR, Doppler, or delay spread. Future work could include extending this approach to multiple-input multiple-output (MIMO) systems, where orthogonal pilots could still be needed to estimate the channel of the different users and compute the equalization and precoding matrices. Another line of work could be the extension of such schemes to other channel models, e.g., with subcarrier interference or no cycle prefix.

## APPENDIX

### A. Derivation of the IEDD baseline

*Derivation of (11):* We denote by  $\text{LLR}_P(k, i)$  the prior information assumed to be available to the estimator for each bit  $i \in \{1, \dots, m\}$  of each resource element  $k \in \{1, \dots, n\}$ . Let  $P_{X_k}$  be the corresponding prior distribution over the transmitted data symbols on the  $k^{\text{th}}$  resource element. For a given constellation point  $c_u \in \mathcal{C}$ ,  $1 \leq u \leq 2^m$ , with corresponding labeling  $(c_u^{(1)}, \dots, c_u^{(m)})$ , with  $c_u^{(i)} \in \{0, 1\}$ ,  $1 \leq i \leq m$ , we have

$$\begin{aligned} \ln(P_{X_k}(c_u)) &= \ln(P(B_{k,1} = c_u^{(1)}, \dots, B_{k,m} = c_u^{(m)})) \\ &= \sum_{i=1}^m \ln(P(B_{k,i} = c_u^{(i)})) \end{aligned} \quad (26)$$

where  $B_{k,i}$  is the random variable corresponding to the  $i^{\text{th}}$  bit transmitted in the  $k^{\text{th}}$  resource element, and (26) is valid assuming the bits mapped to a same resource element are independent. Moreover, we have

$$\begin{aligned} \ln(P(B_{k,i} = 0)) &= -\ln\left(1 + \frac{P(B_{k,i} = 1)}{P(B_{k,i} = 0)}\right) \\ &= -\ln(1 + \exp(\text{LLR}_P(k, i))) \end{aligned} \quad (27)$$

where the last equality comes from the definition of the LLR as  $\text{LLR}_P(k, i) \triangleq \ln\left(\frac{P(B_{k,i}=1)}{P(B_{k,i}=0)}\right)$ . Similarly, we have

$$\ln(P(B_{k,i} = 1)) = \text{LLR}_P(k, i) - \ln(1 + \exp(\text{LLR}_P(k, i))). \quad (28)$$

By combining (26), (27) and (28), we get

$$\ln(P_{X_k}(c_u)) = \sum_{i=1}^m c_u^{(i)} \text{LLR}_P(k, i) - \sum_{i=1}^m \ln(1 + \exp(\text{LLR}_P(k, i))). \quad (29)$$

The second term in the left-hand side of (29) does not depend on  $c_u$ . Therefore, the vector  $\left[\sum_{i=1}^m c_1^{(i)} \text{LLR}_P(k, i), \dots, \sum_{i=1}^m c_{2^m}^{(i)} \text{LLR}_P(k, i)\right]$  corresponds to unscaled log-probabilities, from which the distribution  $P_{X_k}$  can be recovered using the softmax  $(\cdot)$  function:

$$[P_{X_k}(c_1), \dots, P_{X_k}(c_{2^m})] = \text{softmax}\left(\sum_{i=1}^m c_1^{(i)} \text{LLR}_P(k, i), \dots, \sum_{i=1}^m c_{2^m}^{(i)} \text{LLR}_P(k, i)\right) \quad (30)$$

with

$$\text{softmax}(l_1, \dots, l_{2^m}) \triangleq \left[\frac{\exp(l_1)}{\sum_{i=1}^{2^m} \exp(l_i)}, \dots, \frac{\exp(l_{2^m})}{\sum_{i=1}^{2^m} \exp(l_i)}\right]. \quad (31)$$



*Derivation of (12) and (14):* Equations (12) and (14) follow directly from applying the LMMSE estimator. We start by rewriting the OFDM channel transfer function (1) as

$$\mathbf{y} = \text{diag}(\mathbf{x}) \mathbf{h} + \mathbf{w}$$

where  $\mathbf{y} = \text{vec}(\mathbf{Y})$ ,  $\mathbf{x} = \text{vec}(\mathbf{X})$ ,  $\mathbf{h} = \text{vec}(\mathbf{H})$ , and  $\mathbf{w} = \text{vec}(\mathbf{W})$ . We remind that  $\mathbb{E}\{\mathbf{h}\mathbf{h}^H\} = \mathbf{R}$  and  $\mathbb{E}\{\mathbf{w}\mathbf{w}^H\} = \sigma^2 \mathbf{I}_n$ . Moreover, it is assumed that  $x_k$  is distributed according to the prior  $P_{X_k}$ ,  $1 \leq k \leq n$ . The LMMSE channel estimate of  $\mathbf{h}$  is (e.g., [20, Lemma B.17])

$$\hat{\mathbf{h}} = \mathbb{E}\{\mathbf{h}\mathbf{y}^H\} \mathbb{E}\{\mathbf{y}\mathbf{y}^H\}^{-1} \mathbf{y} \quad (32)$$

and the covariance matrix of the estimation error is

$$\tilde{\mathbf{R}} = \mathbb{E}\{\mathbf{h}\mathbf{h}^H\} - \mathbb{E}\{\mathbf{h}\mathbf{y}^H\} \mathbb{E}\{\mathbf{y}\mathbf{y}^H\}^{-1} \mathbb{E}\{\mathbf{y}\mathbf{h}^H\} = \mathbf{R} - \mathbb{E}\{\mathbf{h}\mathbf{y}^H\} \mathbb{E}\{\mathbf{y}\mathbf{y}^H\}^{-1} \mathbb{E}\{\mathbf{y}\mathbf{h}^H\}. \quad (33)$$

Then,

$$\mathbb{E}\{\mathbf{h}\mathbf{y}^H\} = \mathbb{E}\{\mathbf{h}\mathbf{h}^H\} \mathbb{E}\{\mathbf{x}^H\} = \mathbf{R} \text{diag}(\bar{\mathbf{x}})^H \quad (34)$$

where  $\bar{x}_k \triangleq \mathbb{E}\{x_k\}$  with the expectation taken according to the prior  $P_{X_k}$ . Moreover,

$$\begin{aligned} \mathbb{E}\{\mathbf{y}\mathbf{y}^H\} &= \mathbb{E}\left\{(\text{diag}(\mathbf{x}) \mathbf{h})(\text{diag}(\mathbf{x}) \mathbf{h})^H\right\} + \sigma^2 \mathbf{I}_n \\ &= \mathbb{E}\left\{(\mathbf{x} \circ \mathbf{h})(\mathbf{x} \circ \mathbf{h})^H\right\} + \sigma^2 \mathbf{I}_n \\ &= \mathbb{E}\left\{(\mathbf{x}\mathbf{x}^H) \circ (\mathbf{h}\mathbf{h}^H)\right\} + \sigma^2 \mathbf{I}_n \\ &= \mathbb{E}\left\{\mathbf{x}\mathbf{x}^H\right\} \circ \mathbf{R} + \sigma^2 \mathbf{I}_n \end{aligned} \quad (35)$$

and

$$\mathbb{E}\{\mathbf{y}\mathbf{h}^H\} = \text{diag}(\bar{\mathbf{x}}) \mathbf{R}^H. \quad (36)$$

Combining (32), (33), (34), (35), and (36) leads to the desired results:

$$\hat{\mathbf{h}} = \mathbf{R} \text{diag}(\bar{\mathbf{x}})^H (\mathbb{E}\{\mathbf{x}\mathbf{x}^H\} \circ \mathbf{R} + \sigma^2 \mathbf{I}_n)^{-1} \mathbf{y}$$

and

$$\tilde{\mathbf{R}} = \mathbf{R} - \mathbf{R} \text{diag}(\bar{\mathbf{x}})^H (\mathbb{E}\{\mathbf{x}\mathbf{x}^H\} \circ \mathbf{R} + \sigma^2 \mathbf{I}_n)^{-1} \text{diag}(\bar{\mathbf{x}}) \mathbf{R}^H.$$

*Derivation of (15):* Focusing on the  $k^{th}$  resource element,  $1 \leq k \leq n$ , we can rewrite the channel transfer function as

$$y_k = \hat{h}_k x_k + \underbrace{\tilde{h}_k x_k + w_k}_{\tilde{w}_k} \quad (37)$$

where  $w_k \sim \mathcal{CN}(0, \sigma^2)$ ,  $\hat{h}_k$  is the LMMSE estimate of the channel response  $h_k$ , and  $\tilde{h}_k$  the channel estimation error with variance  $\tilde{R}_{k,k}$ . It is assumed that prior information is available on the transmitted bits in the form of LLRs, which for the  $i^{th}$  bit transmitted in the  $k^{th}$  resource element, is denoted by  $\text{LLR}_E(k, i)$ . The transmitted symbols  $X_k$  are assumed to be *a priori* distributed according to a distribution  $\tilde{P}_{X_k}$  computed as in (11) but using the extrinsic information  $\text{LLR}_E$  instead of  $\text{LLR}_P$ . Note that  $\mathbb{E}(\tilde{w}_k \tilde{w}_k^*) = \tilde{R}_{k,k} + \sigma^2$ . Given a constellation point  $c \in \mathcal{C}$  and assuming  $\tilde{w}_k$  is Gaussian distributed we have

$$P(X_k = c | \hat{h}_k, y_k) = \frac{\tilde{P}_{X_k}(c) P(y_k | X_k = c, \hat{h}_k)}{P(y_k | \hat{h}_k)} \quad (38)$$

$$= \frac{\exp\left(-\frac{1}{\tilde{\sigma}_k'^2} |y_k - \hat{h}_k c|^2 + \sum_{i=1}^m c^{(i)} \text{LLR}_E(k, i)\right)}{P(y_k | \hat{h}_k) \pi \tilde{\sigma}_k'^2 \sum_{a \in \mathcal{C}} \exp\left(\sum_{i=1}^m a^{(i)} \text{LLR}_E(k, i)\right)} \quad (39)$$

where  $\tilde{\sigma}_k'^2 = \tilde{R}_{k,k} + \sigma^2$ . Now, we have

$$\begin{aligned} \text{LLR}(k, i) &= \ln \left( \frac{P(B_{k,i} = 1 | \hat{h}_k, y_k)}{P(B_{k,i} = 0 | \hat{h}_k, y_k)} \right) \\ &= \ln \left( \frac{\sum_{c \in \mathcal{C}_{i,1}} P(X_k = c | \hat{h}_k, y_k)}{\sum_{c \in \mathcal{C}_{i,0}} P(X_k = c | \hat{h}_k, y_k)} \right) \\ &= \ln \left( \frac{\sum_{c \in \mathcal{C}_{i,1}} \exp\left(-\frac{1}{\tilde{\sigma}_k'^2} |y_k - \hat{h}_k c|^2 + \sum_{i=1}^m c^{(i)} \text{LLR}_E(k, i)\right)}{\sum_{c \in \mathcal{C}_{i,0}} \exp\left(-\frac{1}{\tilde{\sigma}_k'^2} |y_k - \hat{h}_k c|^2 + \sum_{i=1}^m c^{(i)} \text{LLR}_E(k, i)\right)} \right) \end{aligned} \quad (40)$$

where  $\mathcal{C}_{i,0}(\mathcal{C}_{i,1})$  is the subset of  $\mathcal{C}$  which contains all constellation points with the  $i^{th}$  labeling bit set to 0 (1). A similar expression can be found in [28].

### B. Proof of Proposition 1

We provide here a proof that (19) is an achievable rate assuming some conditions on the channel and receiver hold true. The stochastic process generating the channel response is assumed

to be memoryless and stationary. By stationary, we mean that for any couple of indexes  $(i, k)$ ,  $\mathbb{E}\{h_i\} = \mathbb{E}\{h_k\}$ ,  $\mathbb{E}\{h_i h_k^*\} = \mathbb{E}\{h_{i-k} h_0^*\}$ , and  $\mathbb{E}\{|h_i|^2\} < \infty$ . The channel model presented in Section II-A is both memoryless and stationary. Moreover, by achievable rate, we mean according to the standard definition [21, §8.5].

We leverage the random coding argument. We aim to transmit a message randomly chosen from a set  $\{1, \dots, 2^u\}$ , where  $u$  is an integer. Each resource element takes as input  $m$  bits, and a frame is formed of  $n$  resource elements, among which a set  $\mathcal{N}_D$  of size  $n_D$  can be used to transmit data. A code  $\mathcal{B}$  is constructed by generating  $2^u$  binary codewords of length  $vn_D m$  denoted by  $\mathbf{b}$ , where  $v$  is the number of frames over which a codeword spreads.<sup>3</sup> Codewords are generated by independently and uniformly drawing bits. A message  $w \in \{1, \dots, 2^u\}$  is encoded at the transmitter by mapping it to a codeword  $\mathbf{b}(w) \in \mathcal{B}$  in a manner known to the receiver. For convenience, bits forming a codeword  $\mathbf{b}$  are indexed by  $b_{l,k,i}$  to refer to the  $i^{\text{th}}$  bit on the  $k^{\text{th}}$  resource element of the  $l^{\text{th}}$  frame.

On the receiver side, reconstruction of the transmitted codeword is achieved using for each bit  $i$  and resource element  $k$  a non-negative decoding metric that jointly operates on the  $n_D$  data carrying resource elements of a frame of received symbols taken from the channel output alphabet. This metric is denoted by  $q_{k,i}(b, \mathbf{y})$  where  $b$  is either 0 or 1, and  $\mathbf{y}$  is a vector of received data symbols of length  $n_D$  corresponding to a single frame. Decoding is performed by selecting the codeword  $\hat{w}$  such that

$$\hat{w} = \arg \max_w \left( \prod_{l=1}^v \prod_{k \in \mathcal{N}_D} \prod_{i=1}^m q_{k,i}(b_{l,k,i}(w), \mathbf{y}_l) \right) \quad (41)$$

where  $\mathbf{y}_l$  is the vector of channel output symbols corresponding to the  $l^{\text{th}}$  frame. We introduce for convenience

$$\bar{q}(\mathbf{b}, \mathbf{y}) \triangleq \prod_{l=1}^v \prod_{k \in \mathcal{N}_D} \prod_{i=1}^m q_{k,i}(b_{l,k,i}, \mathbf{y}_l). \quad (42)$$

Following the approach adopted in [29], [30], we fix the transmitted message to  $w$ , the channel input  $\mathcal{X}$  to  $\mathbf{b}(w)$ , and the channel output  $\mathcal{Y}$  to  $\mathbf{y} = [\mathbf{y}_1, \dots, \mathbf{y}_v]$ , and compute the probability that a decoding error occurs, i.e.,

$$P(E | \mathcal{X} = \mathbf{b}(w), \mathcal{Y} = \mathbf{y}) = P \left( \bigcup_{w' \neq w} [\bar{q}(\mathbf{b}(w'), \mathbf{y}) \geq \bar{q}(\mathbf{b}(w), \mathbf{y})] \middle| \mathcal{X} = \mathbf{b}(w), \mathcal{Y} = \mathbf{y} \right). \quad (43)$$

<sup>3</sup>A codeword is contained in a single frame in most practical systems. However, for the sake of this proof, we allow a codeword to spread over multiple frames.

Note that randomness comes from the random construction of the code  $\mathcal{B}$ . We have

$$P(E|\mathcal{X} = \mathbf{b}(w), \mathcal{Y} = \mathbf{y}) \leq \sum_{w' \neq w} P(\bar{q}(\mathbf{b}(w'), \mathbf{y}) \geq \bar{q}(\mathbf{b}(w), \mathbf{y}) | \mathcal{X} = \mathbf{b}(w), \mathcal{Y} = \mathbf{y}) \quad (44)$$

$$\leq \frac{1}{\bar{q}(\mathbf{b}(w), \mathbf{y})} \sum_{w' \neq w} \mathbb{E}_{\mathcal{B}} \{\bar{q}(\mathbf{b}(w'), \mathbf{y}) | \mathcal{Y} = \mathbf{y}\} \quad (45)$$

$$\leq \frac{2^u}{\bar{q}(\mathbf{b}(w), \mathbf{y})} \mathbb{E}_{\mathbf{b}} \{\bar{q}(\mathbf{b}, \mathbf{y}) | \mathcal{Y} = \mathbf{y}\} \quad (46)$$

$$\leq 2^u \frac{\mathbb{E}_{\mathbf{b}} \{\prod_{l=1}^v \prod_{k \in n_D} \prod_{i=1}^m q_{k,i}(b_{l,k,i}, \mathbf{y}_l) | \mathcal{Y} = \mathbf{y}\}}{\prod_{l=1}^v \prod_{k \in n_D} \prod_{i=1}^m q_{k,i}(b_{l,k,i}(w), \mathbf{y}_l)} \quad (47)$$

$$\leq 2^u \prod_{l=1}^v \prod_{k \in n_D} \prod_{i=1}^m \frac{\mathbb{E}_{b_{l,k,i}} \{q_{k,i}(b_{l,k,i}, \mathbf{y}_l)\}}{q_{k,i}(b_{l,k,i}(w), \mathbf{y}_l)} \quad (48)$$

where (44) follows from the union bound, (45) follows from the Markov inequality, (46) follows from the uniformly and independently drawn codewords, (47) follows from (42), and (48) follows from the assumption that bits forming codewords are independently and uniformly drawn. We can rewrite (48) as

$$P(E|\mathcal{X} = \mathbf{b}(w), \mathcal{Y} = \mathbf{y}) \leq 2^{-v(T_v - R_c)} \quad (49)$$

where  $R_c \triangleq \frac{u}{v}$  is the rate [bit frame<sup>-1</sup>] and

$$T_v(w, \mathbf{y}) \triangleq \frac{1}{v} \sum_{l=1}^v \sum_{k \in n_D} \sum_{i=1}^m \log_2 \left( \frac{q_{k,i}(b_{l,k,i}(w), \mathbf{y}_l)}{\mathbb{E}_{b_{l,k,i}} \{q_{k,i}(b_{l,k,i}, \mathbf{y}_l)\}} \right) \quad (50)$$

$$= n_D m + \sum_{k \in n_D} \sum_{i=1}^m \frac{1}{v} \sum_{l=1}^v \log_2 \left( \frac{q_{k,i}(b_{l,k,i}(w), \mathbf{y}_l)}{q_{k,i}(0, \mathbf{y}_l) + q_{k,i}(1, \mathbf{y}_l)} \right). \quad (51)$$

One can notice that

$$Q_{k,i}(b|\mathbf{y}_l) \triangleq \frac{q_{k,i}(b, \mathbf{y}_l)}{q_{k,i}(0, \mathbf{y}_l) + q_{k,i}(1, \mathbf{y}_l)} \quad (52)$$

forms a probability mass function over the two possible outcomes of the  $i^{th}$  bit carried by the  $k^{th}$  resource element. Because the codewords are generated by independently and uniformly drawing bits and because the channel is assumed to be stationary, the  $\mathbf{y}_l$ ,  $1 \leq l \leq v$  are independent and identically distributed (i.i.d.). Therefore, for a given couple of indexes  $(k, i)$ , the  $Q_{k,i}(b, \mathbf{y}_l)$ ,  $1 \leq l \leq v$  are also i.i.d.. Hence, we can apply the weak law of large numbers:

$$\lim_{v \rightarrow \infty} P \left( \frac{1}{v} \sum_{l=1}^v \log_2 (Q_{k,i}(b_{l,k,i} | \mathbf{y}_l)) = \mathbb{E}_{\mathbf{y}', b_{k,i}} \{\log_2 (Q_{k,i}(b_{k,i} | \mathbf{y}'))\} \right) = 1. \quad (53)$$

Note that randomness comes from random drawing of  $b_{l,k,i}$  and  $\mathbf{y}_l$ . Therefore, for any couple of positive real numbers  $(\delta, \epsilon)$ , there exists  $v$  large enough such that, with probability at least  $1 - \epsilon$ ,

$$\frac{1}{v} \sum_{l=1}^v \log_2 (Q_{k,i} (b_{l,k,i} | \mathbf{y}_l)) \geq \mathbb{E}_{\mathbf{y}', b_{k,i}} \{ \log_2 (Q_{k,i} (b_{k,i} | \mathbf{y}')) \} - \frac{\delta}{n_D m} \quad (54)$$

which, when combined with (49) and (51), leads from the union bound to

$$P(E) \leq 2^{-v(n_D m + \sum_{k \in n_D} \sum_{i=1}^m \mathbb{E}_{\mathbf{y}', b_{k,i}} \{ \log_2 (Q_{k,i} (b_{k,i} | \mathbf{y}')) \} - \delta - R_c)} + \epsilon. \quad (55)$$

One can conclude from this result that

$$R \triangleq n_D m + \sum_{k \in n_D} \sum_{i=1}^m \mathbb{E}_{\mathbf{y}', b_{k,i}} \{ \log_2 (Q_{k,i} (b_{k,i} | \mathbf{y}')) \} \quad (56)$$

is an achievable rate, i.e., for any  $R_c < R$ , the probability of error can be made arbitrarily low.

$R$  can be rewritten as

$$R = \sum_{k \in n_D} \sum_{i=1}^m I(B_{k,i}, \mathcal{Y}) - \sum_{k \in n_D} \sum_{i=1}^m \mathbb{E}_{\mathbf{y}'} \{ \mathbf{D}_{\text{KL}} (P_{B_{k,i}}(\cdot | \mathbf{y}') || Q_{k,i}(\cdot | \mathbf{y}')) \} \quad (57)$$

where  $P_{B_{k,i}}(\cdot | \mathbf{y})$  is the true posterior distribution on the  $i^{\text{th}}$  bit transmitted on the  $k^{\text{th}}$  resource element conditioned on  $\mathbf{y}$ .

## REFERENCES

- [1] J. Downey, B. Hilburn, T. O'Shea, and N. West, "Machine Learning Remakes Radio," *IEEE Spectrum*, vol. 57, no. 5, pp. 35–39, 2020.
- [2] D. Gündüz, P. de Kerret, N. D. Sidiropoulos, D. Gesbert, C. R. Murthy, and M. van der Schaar, "Machine Learning in the Air," *IEEE J. Sel. Areas Commun.*, vol. 37, no. 10, pp. 2184–2199, 2019.
- [3] M. Stark, F. Ait Aoudia, and J. Hoydis, "Joint Learning of Geometric and Probabilistic Constellation Shaping," in *Proc. IEEE Globecom Workshops (GC Wkshps)*, 2019.
- [4] S. Cammerer, F. Ait Aoudia, S. Dörner, M. Stark, J. Hoydis, and S. T. Brink, "Trainable Communication Systems: Concepts and Prototype," *IEEE Trans. Commun.*, 2020.
- [5] T. O'Shea and J. Hoydis, "An Introduction to Deep Learning for the Physical Layer," *IEEE Trans. Cogn. Commun. Netw.*, vol. 3, no. 4, pp. 563–575, Dec. 2017.
- [6] Z. Zhu, J. Zhang, R. Chen, and H. Yu, "Autoencoder-Based Transceiver Design for OWC Systems in Log-Normal Fading Channel," *IEEE Photon. J.*, vol. 11, no. 5, pp. 1–12, Oct. 2019.
- [7] B. Karanov, M. Chagnon, F. Thouin, T. A. Eriksson, H. Bülow, D. Lavery, P. Bayvel, and L. Schmalen, "End-to-End Deep Learning of Optical Fiber Communications," *J. Lightw. Technol.*, vol. 36, no. 20, pp. 4843–4855, Oct. 2018.
- [8] S. Dörner, S. Cammerer, J. Hoydis, and S. ten Brink, "Deep Learning Based Communication Over the Air," *IEEE J. S. Topics in Signal Process.*, vol. 12, no. 1, pp. 132–143, Feb 2018.
- [9] H. Ye, G. Y. Li, and B. Juang, "Power of Deep Learning for Channel Estimation and Signal Detection in OFDM Systems," *IEEE Wireless Commun. Lett.*, vol. 7, no. 1, pp. 114–117, 2018.

- [10] M. Honkala, D. Korpi, and J. M. Huttunen, "DeepRx: Fully Convolutional Deep Learning Receiver," *preprint arXiv:2005.01494*, 2020.
- [11] A. Felix, S. Cammerer, S. Dörner, J. Hoydis, and S. Ten Brink, "OFDM-Autoencoder for End-to-End Learning of Communications Systems," in *IEEE Int. Workshop on Signal Process. Advances in Wireless Commun. (SPAWC)*, 2018.
- [12] M. Kim, W. Lee, and D. Cho, "A Novel PAPR Reduction Scheme for OFDM System Based on Deep Learning," *IEEE Commun. Lett.*, vol. 22, no. 3, pp. 510–513, 2018.
- [13] E. Balevi and J. G. Andrews, "One-Bit OFDM Receivers via Deep Learning," *IEEE Trans. Commun.*, vol. 67, no. 6, pp. 4326–4336, 2019.
- [14] T. Y. Al-Naffouri, A. A. Dahman, M. S. Sohail, W. Xu, and B. Hassibi, "Low-Complexity Blind Equalization for OFDM Systems With General Constellations," *IEEE Trans. Signal Processing*, vol. 60, no. 12, pp. 6395–6407, 2012.
- [15] A. Saci, A. Al-Dweik, A. Shami, and Y. Iraqi, "One-Shot Blind Channel Estimation for OFDM Systems Over Frequency-Selective Fading Channels," *IEEE Trans. Commun.*, vol. 65, no. 12, pp. 5445–5458, 2017.
- [16] G. Taricco, "On the Convergence of Multipath Fading Channel Gains to the Rayleigh Distribution," *IEEE Wireless Commun. Lett.*, vol. 4, no. 5, pp. 549–552, 2015.
- [17] R. W. Heath Jr and A. Lozano, *Foundations of MIMO communication*. Cambridge University Press, 2018.
- [18] R. H. Clarke, "A Statistical Theory of Mobile-Radio Reception," *Bell Syst. Tech. J.*, vol. 47, no. 6, pp. 957–1000, 1968.
- [19] F. Sanzi, Sven Jelting, and J. Speidel, "A Comparative Study of Iterative Channel Estimators for Mobile OFDM Systems," *IEEE Trans. on Wireless Commun.*, vol. 2, no. 5, pp. 849–859, 2003.
- [20] E. Björnson, J. Hoydis, and L. Sanguinetti, "Massive MIMO networks: Spectral, energy, and hardware efficiency," *Foundations and Trends® in Signal Processing*, vol. 11, no. 3-4, pp. 154–655, 2017.
- [21] T. M. Cover, *Elements of Information Theory*. John Wiley & Sons, 1999.
- [22] F. Ait Aoudia and J. Hoydis, "Model-Free Training of End-to-End Communication Systems," *IEEE J. Sel. Areas Commun.*, vol. 37, no. 11, pp. 2503–2516, Nov 2019.
- [23] M. Soltani, V. Pourahmadi, and H. Sheikhzadeh, "Pilot Pattern Design for Deep Learning-Based Channel Estimation in OFDM Systems," *preprint arXiv:2003.08980*, 2020.
- [24] M. Boloursaz Mashhadi and D. Gunduz, "Pruning the Pilots: Deep Learning-Based Pilot Design and Channel Estimation for MIMO-OFDM Systems," *preprint arXiv:2006.11796*, 2020.
- [25] X. Ma and Z. Gao, "Data-Driven Deep Learning to Design Pilot and Channel Estimator for Massive MIMO," *IEEE Trans. on Veh. Technol.*, vol. 69, no. 5, pp. 5677–5682, 2020.
- [26] K. He, X. Zhang, S. Ren, and J. Sun, "Deep Residual Learning for Image Recognition," in *Proc. IEEE Conf. on Comput. Vision and Pattern Recognit. (CVPR)*, June 2016.
- [27] "IEEE Standard for Information technology – Local and metropolitan area networks – Specific requirements – Part 11: Wireless LAN Medium Access Control (MAC) and Physical Layer (PHY) Specifications," *IEEE Std 802.11n-2009*, Oct. 2009.
- [28] S. ten Brink, J. Speidel, and Ran-Hong Yan, "Iterative Demapping and Decoding for Multilevel Modulation," in *Proc. IEEE Globecom Conf.*, 1998, pp. 579–584.
- [29] G. Böcherer, "Achievable Rates for Probabilistic Shaping," *preprint arXiv:1707.01134*, 2017.
- [30] Y. Lomnitz and M. Feder, "A Simpler Derivation of the Coding Theorem," *preprint arXiv:1205.1389*, 2012.